

The Crystal Structure of the C-Terminal DAP5/p97 Domain Sheds Light on the Molecular Basis for Its Processing by Caspase Cleavage

Noa Liberman¹, Orly Dym², Tamar Unger², Shira Albeck², Yoav Peleg², Yossi Jacobovitch², Anna Branzburg², Miriam Eisenstein³, Lea Marash¹ and Adi Kimchi^{1*}

¹Department of Molecular Genetics, Weizmann Institute of Science, Rehovot 76100, Israel

²Department of Structural Biology, The Israel Structural Proteomics Center, Weizmann Institute of Science, Rehovot 76100, Israel

³Chemical Research Support, Weizmann Institute of Science, Rehovot 76100, Israel

Received 3 June 2008;
received in revised form
31 July 2008;
accepted 5 August 2008
Available online
12 August 2008

DAP5/p97 (death-associated protein 5) is a member of the eukaryotic translation initiation factor 4G family. It functions as a scaffold protein promoting cap-independent translation of proteins. During apoptosis, DAP5/p97 is cleaved by caspases at position 792, yielding an 86-kDa C-terminal truncated isoform (DAP5/p86) that promotes translation of several mRNAs mediated by an internal ribosome entry site. In this study, we report the crystal structure of the C-terminal region of DAP5/p97 extending between amino acids 730 and 897. This structure consists of four HEAT-Repeats and is homologous to the C-terminal domain of eIF4GI, eIF5, and eIF2B ϵ . Unlike the other proteins, DAP5/p97 lacks electron density in the loop connecting α 3 and α 4, which harbors the caspase cleavage site. Moreover, we observe fewer interactions between these two helices. Thus, previous mapping of this site by mutation analysis is confirmed here by the resolved structure of the DAP5/p97 C-terminus. In addition, we identified the position of two conserved aromatic and acidic boxes in the structure of the DAP5/p97 C-terminus. The acidic residues in the two aromatic and acidic boxes form a continuous negatively charged patch, which is suggested to make specific interactions with other proteins such as eIF2B. The caspase cleavage of DAP5/p97 removes the subdomain carrying acidic residues in the AA-box motif, which may result in exposure of a hydrophobic surface. These intriguing structural differences between the two DAP5 isoforms suggest that they have different interaction partners and, subsequently, different functions.

© 2008 Elsevier Ltd. All rights reserved.

Edited by R. Huber

Keywords: protein translation; DAP5; caspase; AA boxes; HEAT-Repeat

Introduction

Initiation of translation in eukaryotes is a highly regulated process. The majority of initiation events in the cell occur through a cap-dependent mechanism. This mode of initiation involves the assembly of the preinitiation complex at the mRNA 5'Cap m⁷GpppX structure. The preinitiation complex

consists of several initiation factors including, among others, the ternary complex of eukaryotic translation initiation factor (eIF) 4E, eIF4A, and eIF4G. eIF4E is a protein that specifically recognizes the cap structure,^{1,2} eIF4A is an ATP-dependent RNA helicase that serves to unwind secondary structures within the 5' untranslated region (UTR) of the mRNA,^{2,3} and eIF4G is a scaffold protein that bridges eIF4E and eIF4A. In addition, eIF4G recruits eIF3, which in turn interacts with the small ribosomal subunit. eIF4G also binds the poly(A)-binding protein, allowing circularization of the mRNA and as well as the Mnk1 protein kinase that phosphorylates eIF4E in these complexes.^{4,5}

An alternative mechanism of translation initiation involves the recruitment of the ribosome to the

*Corresponding author. E-mail address:
adi.kimchi@weizmann.ac.il.

Abbreviations used: eIF, eukaryotic translation initiation factor; UTR, untranslated region; IRES, internal ribosome entry site; AA box, aromatic and acidic box; HR, HEAT-Repeat.

mRNA at a position close to or directly at the initiator codon. This mode of initiation requires the presence of an internal ribosome entry site (IRES) element within the mRNA's 5'UTR, which, by interacting with the translation machinery, enables ribosome binding independent of the 5'Cap structure. The cap-dependent mechanism of initiation is frequently blocked by various cellular stresses. A characteristic of IRES-mediated translation initiation is its ability to proceed under conditions in which cap-dependent translation is inhibited.⁶⁻⁸

DAP5/p97 (*death-associated protein 5*), a member of the eIF4G protein family,^{9,10} has been implicated in mediating cap-independent translation. The homology of DAP5/p97 to eIF4G is largely confined to the central segment, which corresponds to the eIF4A and eIF3 binding regions.¹⁰⁻¹³ The N-terminal part of eIF4G that contains the binding sites for eIF4E and poly(A)-binding protein is completely missing from DAP5/p97.^{10,11,14-16} Consistent with sequence data, it was shown that DAP5/p97 indeed binds eIF3 and eIF4A, while it fails to bind eIF4E necessary for cap-dependent translation.^{11,14,16-19} The C-terminal parts of eIF4G and DAP5/p97 contain two aromatic and acidic boxes (AA boxes) (aromatic/aliphatic and acidic residues; also known as eIF5C or W2 domain).²⁰⁻²³ Notably, both eIF4G and DAP5/p97 bind to Mnk1 using the AA-box motif. In contrast, DAP5/p97, but not eIF4G, binds to eIF2 β through the AA-box motif.²⁴ eIF2 β is a subunit of the adaptor protein eIF2, which brings the initiator Met-tRNA to the preinitiation complex. The differential binding of eIF2 β suggests that functional differences between DAP5/p97 and eIF4G may also reside in their C-terminal regions, in addition to the abovementioned differences in the N-terminal region.

DAP5/p97 was identified and cloned simultaneously by four independent groups.^{11,16,25,26} In our laboratory, DAP5/p97 was isolated through a genetic screen aimed at identifying novel prodeath genes essential for interferon- γ -induced cell death.¹⁶ While this protein was being studied as part of the cell death process, it was revealed that, under apoptotic conditions, DAP5/p97 undergoes proteolytic cleavage, giving rise to a 86-kDa fragment (DAP5/p86). By using a panel of inhibitors for various cellular proteases, the cleavage of DAP5/p97 was attributed to caspases. Examination of the amino acid sequence of DAP5/p97 revealed the existence of two potential caspase cleavage sites of the motif DXXD (DETD⁷⁹² and DHVD⁸²⁵), which are capable of yielding a cleavage product that is close to the expected size. DAP5/p97 mutants carrying a single substitution of the aspartic residue with alanine (DXXD \rightarrow DXXA) in both potential sites were constructed, and the ability of each mutation to abolish the cleavage site upon death stimulus was examined. This work revealed that DAP5/p97 was converted into DAP5/p86 by a single caspase cleavage event at DETD⁷⁹², whereas the second potential DHVD⁸²⁵ site was silent. The cleavage at D792 generated an isoform of the protein lacking the last 115 C-terminal amino acids.¹⁸

Subsequently, it was demonstrated, either by ectopically expressing DAP5/p86 in cells²⁷⁻²⁹ or by adding the recombinant isoform to cell-free systems,²⁷ that the cleaved isoform is more active than the full-length protein in promoting the IRES-driven translation of some mRNAs coding for apoptotic-related genes. In addition, it was shown that the 5'UTR of the DAP5/p97 mRNA itself fulfils the set of criteria defining an IRES element, and that DAP5/p97 is capable of supporting translation from its own IRES in dying cells.¹⁸ These DAP5/p86-mediated activities are considered to be part of the cellular response during apoptotic cell death manifested when cap-dependent translation is compromised.⁹ In recent years, DAP5/p97 protein has also been found to display positive effects on translation, promoting the IRES-driven translation of target mRNAs and enhancing general uncapped mRNA translation in reconstituted cell-free systems.³⁰⁻³² In addition, it has been demonstrated that endogenous DAP5/p97 cosediments with polysomes in sucrose gradients, suggesting that it is actively involved in translation even at steady-state growth conditions.^{24,33} Recent work, based on knocking down DAP5/p97 in unstressed HeLa cells, established that the full-length protein promotes the cap-independent translation of mRNAs encoding two prosurvival proteins, Bcl-2 and CDK1. The depletion of DAP5/p97 from cells and the resulting decline in the expression of Bcl-2 and CDK1 caused caspase-dependent cell death that was most prominent in the mitotic phase of the cell cycle.³⁴ Although both DAP5 isoforms display important roles in protein translation, the detailed functional differences between the two have not been established yet. This further stresses the importance of crystallizing the C-terminal domain of DAP5/p97 harboring the caspase cleavage site. Moreover, comparison with the existing structure of the close family member eIF4G should highlight the unique functions of DAP5/p97 in light of its rising importance in the regulation of translation during cell death/survival processes.

In this study, we report the crystal structure of the C-terminal region of DAP5/p97 extending between amino acids 730 and 897 (designated as DAP5-CTD). This structure belongs to the subclass of proteins containing HEAT-Repeat (HR) domains that include eIF4GI, eIF5, and eIF2B ϵ , all of which contain AA-box motifs.^{22,23,35} The first AA box of DAP5-CTD consists of helices $\alpha 6$ and $\alpha 7$, whereas the second motif begins at the C-terminal half of $\alpha 8$ and extends until residue 900. The AA boxes, which are rich in acidic residues, form a continuous negatively charged patch that was shown to interact with the positively charged segments of Mnk1 and eIF2 β . The structure of DAP5-CTD is similar to those of eIF4GI, eIF5, and eIF2B ϵ , with the exception of the loop connecting $\alpha 3$ to $\alpha 4$, which lacks electron density in DAP5-CTD. The sequence of this loop is considerably longer in DAP5-CTD and includes the established caspase cleavage site at position D792. Following cleavage at this site, the

negatively charged C-terminal characteristic of the full-length protein is removed, exposing a hydrophobic surface that may imply new interactions for DAP5/p86. Thus, previous biochemical studies that mapped the caspase cleavage site by mutagenesis¹⁸ are in line with the resolved structure of DAP5-CTD, which shows that the position of the site allows access to caspases and predicts the removal of the cleaved fragment with its associated structural domains.

Results and Discussion

Structural overview of DAP5-CTD

In this study, we present the crystal structure of a C-terminal domain of human DAP5/p97, DAP5-CTD, between residues L730 and A897 (Fig. 1). The last stretch of amino acids (899–907) was omitted from the construct due to its predicted unstructured

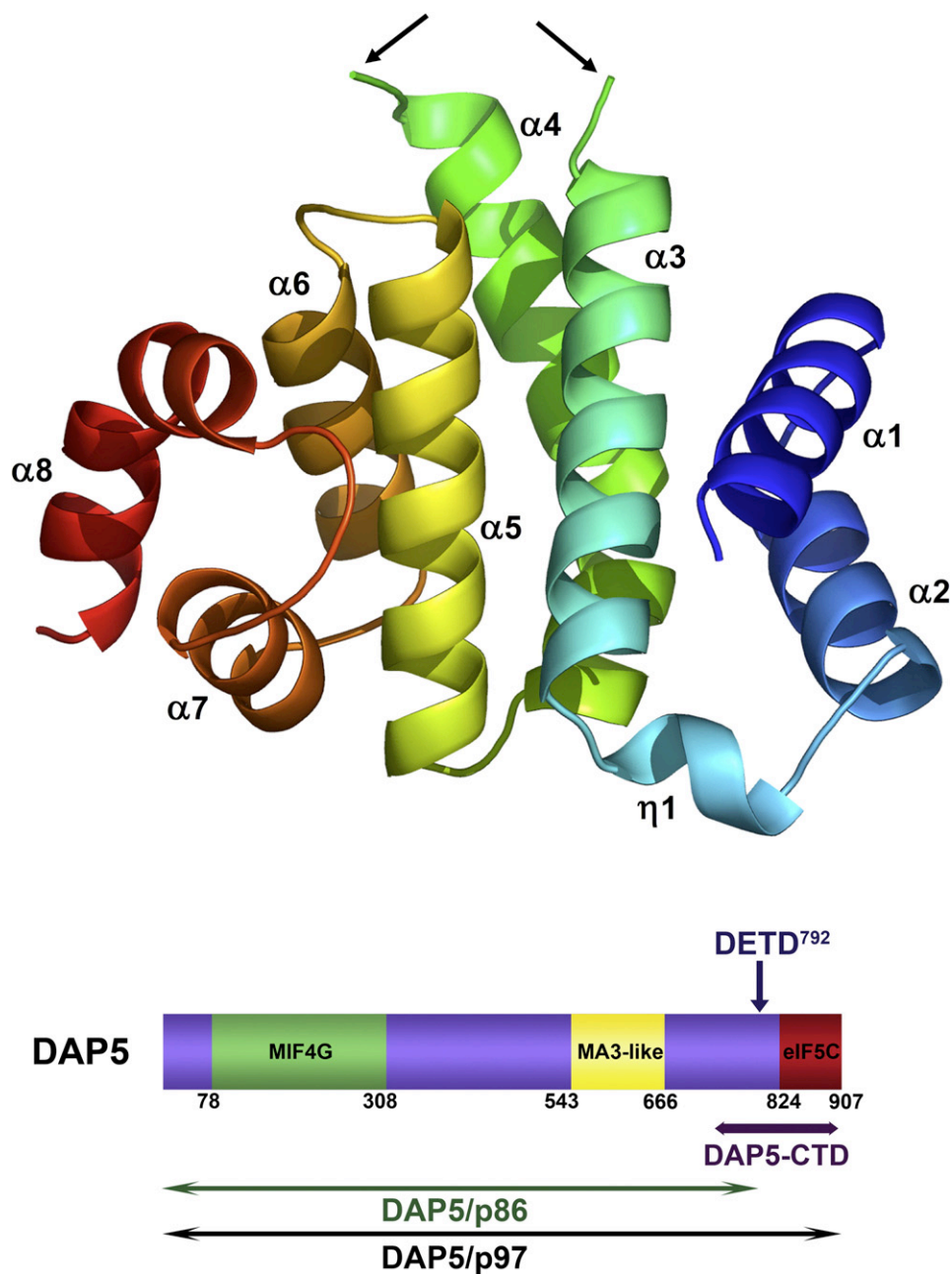


Fig. 1. DAP5-CTD structure (730–897). Top: Ribbon representation of DAP5-CTD. The structure is composed of eight helices (rainbow representation according to order) that fold into four HRs $\alpha 1\alpha 2$, $\alpha 3\alpha 4$, $\alpha 5\alpha 6$, and $\alpha 7\alpha 8$. The boundaries of the segment with missing electron density (residues 789–795), which includes the caspase cleavage site between $\alpha 3$ and $\alpha 4$, are depicted by arrows. Bottom: Scheme presenting the functional domains of DAP5. The boundaries of the domains have been determined according to UniProt Knowledgebase entry P78344. DAP5-CTD is marked by a purple line. The caspase cleavage site is marked in blue. DAP5/p97 and DAP/p86 are marked by black and green lines, respectively.

Table 1. Summary of multiple-wavelength anomalous diffraction data collection from crystals of selenomethionine DAP5-CTD

	Peak	Remote
<i>Data collection</i>		
Resolution range (Å) ^a	25.0–1.9 (1.97–1.90)	23.0–1.85 (1.92–1.85)
λ (Å)	0.979	0.9814
Space group	<i>P</i> ₂ ₁	
Unit cell dimensions (Å)		
<i>a</i>	61.06	
<i>b</i>	45.73	
<i>c</i>	63.36	
Number of molecules in the asymmetric unit	2	
Number of reflections measured	203,573	110,027
Number of unique reflections ^a	27,035 (2682)	29,276 (2916)
<i>R</i> _{sym} ^{a,b}	0.068 (0.333)	0.051 (0.376)
Completeness (%) ^a	100.0 (100.0)	99.8 (100.0)
Redundancy	7.5 (7.5)	3.8 (3.8)
⟨ <i>I</i> ⟩/⟨σ(<i>I</i>)⟩	47.8 (5.8)	33.7 (3.1)
<i>Refinement statistics</i>		
Resolution limits (Å)	23.0–1.9	
<i>R</i> _{free} ^c (%)	25.9	
<i>R</i> _{work} ^c (%)	21.2	
Mean <i>B</i> -factor (Å ²)	30.53	
rmsd (Å)	0.019	
Bond angles (°)	1.73	
Torsion angles (°)	6.01	
Ramachandran plot (%)		
Most favored regions	93.7	
Additional favored regions	6.3	
Generously allowed regions	0.0	
Disallowed regions	0.0	

^a Values in parentheses are for the highest-resolution shells.

^b $R_{\text{sym}} = \sum | \langle I_{hkl} \rangle - I_{hkl} | / I_{hkl}$, where $\langle I_{hkl} \rangle$ is the average intensity over symmetry-related reflections and I_{hkl} is the observed intensity.

^c $R = \sum ||F_o| - |F_c|| / \sum |F_o|$, where F_o denotes the observed structure factor amplitude and F_c denotes the structure factor calculated from the model.

character (FoldIndex³⁶). The N-terminal boundary was selected based on sequence similarity to the structure of eIF4G (4G/C2) [Protein Data Bank (PDB) code 1UG3]. DAP5-CTD crystallizes with two independent monomers per asymmetric unit (crystallization and refinement data are summarized in Table 1). Each monomer forms a globular α -helical HR domain consisting of eight helices, which fold into four HRs $\alpha 1\alpha 2$, $\alpha 3\alpha 4$, $\alpha 5\alpha 6$, and $\alpha 7\alpha 8$ (Fig. 1). Each HR unit consists of a pair of interacting antiparallel helices linked by a flexible interunit loop. This fold is implicated in protein–protein interactions such as in eIF4GI²² and in the extra-catalytic domains of ATR, ATM, and TOR families.³⁷

Comparison of the DAP5-CTD to other translation initiation factors

Three proteins involved in translation initiation—eIF5, eIF2B ϵ , and eIF4GI—were shown to contain HR domains in their C-terminus.^{22,23,35} eIF5 is a GTPase-activating protein specific for eIF2, and

eIF2B is the guanine nucleotide exchange factor specific for eIF2.³⁸ Here we show that DAP5-CTD, another translation initiation factor, contains four HR repeats as well. A sequence and structure comparison of the C-terminal domains of human DAP5/p97 (DAP-CTD; PDB code 3D3M), yeast eIF2B ϵ (eIF2B ϵ -CTD; PDB code 1PAQ), human eIF4GI (eIF4GI-CTD; PDB code 1UG3), and human eIF5 (eIF5-CTD; PDB code 2IU1) is presented in Fig. 2. This alignment is based on structural alignments that were performed manually by superposing each of the structures to DAP5-CTD in turn. The overlaid structures show that the segments, including helices $\alpha 5$ – $\alpha 8$, superpose well in all four structures, whereas helices $\alpha 1$ – $\alpha 4$ vary to a larger extent. Notably, the most conserved sequence stretches include the two conserved AA-box motifs that are within the structurally conserved $\alpha 5$ – $\alpha 8$ segment (Fig. 2). All in all, the proteins share a similar structural fold at their C-terminus despite the fact that they have different functions in translation initiation. While DAP5/p97 and eIF4GI function as scaffold proteins of initiation complexes, eIF2B and eIF5 modulate the activity of eIF2. This is another example where similar structural domains are utilized for different biochemical functions.

AA-box motifs in DAP5-CTD

The most conserved region in the C-terminal domain of all four proteins (DAP5/p97, eIF2B ϵ , eIF5, and eIF4GI) lies in the two AA-box motifs^{20,22,23} (AA1 and AA2 in Fig. 2). In DAP5-CTD, AA1 extends from L848 to W869, while AA2 extends from W890 to E900 (our construct was taken until E898). Both AA boxes are composed of an aromatic/aliphatic motif, followed by a stretch of acidic residues (Fig. 2). These acidic residues (E859, E862, E863, E864, E871, D872, and E895), together with exposed residues from a loop connecting $\alpha 4$ and $\alpha 5$ (D822 and D825), form a negatively charged patch (Fig. 3). Interestingly, only nine residues in this C-terminal region are conserved among these four proteins, all of which are part of the two AA boxes, thus further stressing the importance of this motif.

AA-box motifs are known to mediate specific binding to positively charged segments of proteins. In the case of DAP5/p97 and eIF4GI, this motif was shown to be involved in the binding of Mnk1.^{4,5} This interaction is mediated by a single stretch of eight basic amino acids (RK box) at the Mnk1 N-terminus. The AA-box motif was also shown to mediate binding to eIF2 β ^{20,21,23,24} in the case of DAP5/p97, eIF5, and eIF2B ϵ , utilizing three stretches of seven lysine residues (K boxes) at the eIF2 β N-terminus. For DAP5/p97, this interaction was shown by mutations of the four Glu residues 898–901 to Ala (in the AA2 box) that resulted in reduced binding to eIF2 β .²⁴ Both AA boxes were shown to be important in eIF5's interaction with eIF2 β .³⁹ Interestingly, eIF4GI does not bind eIF2 β ,²⁴ as opposed to DAP5/p97, eIF5, and eIF2B ϵ . Therefore, we searched for residues that will distinguish eIF4GI from the three other proteins.

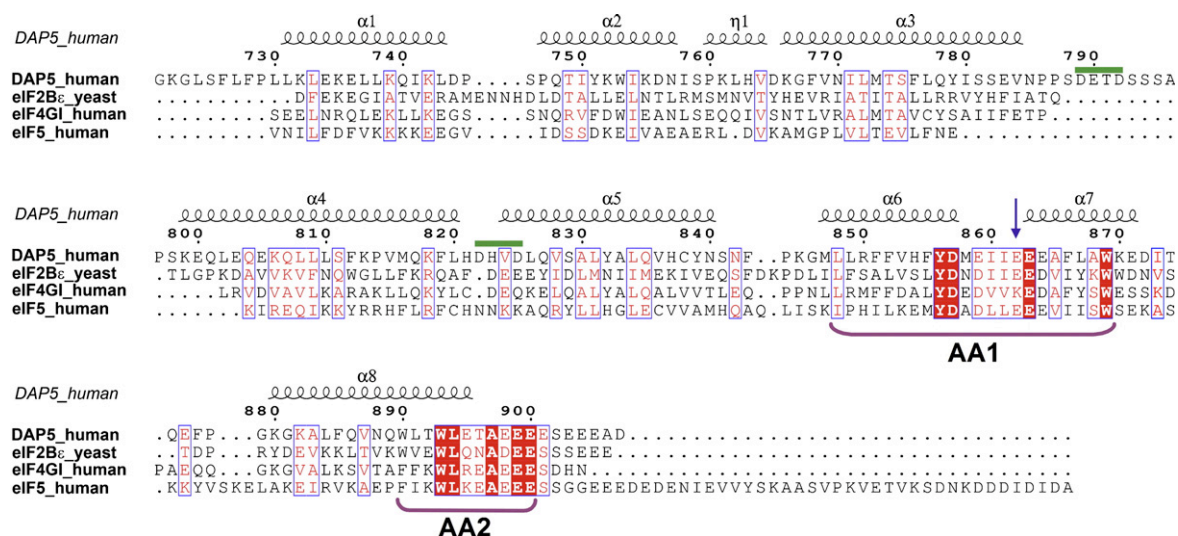


Fig. 2. Structure-based sequence alignment of DAP5/p97, eIF4GI, eIF2B ϵ , and eIF5 C-termini. C-terminal domains of human DAP5/p97 (DAP5-CTD) (residues 730–897; PDB code 3D3M), yeast eIF2B ϵ (residues 549–712; PDB code 1PAQ), human eIF4GI (residues 1441–1590; PDB code 1UG3), and human eIF5 (residues 240–430; PDB code 2IU1) are presented. Numbering and secondary structural elements are presented according to the structure of DAP5-CTD. All α -helices are spirals and labeled above the corresponding sequence. The residues conserved in all four proteins are highlighted in red, and similar residues are in blue boxes. The caspase recognition sites DETD⁷⁹² and DHVD⁸²⁵ are indicated by a green line. The two conserved AA motifs, AA1 and AA2, are marked in purple. The blue arrow points to residue E862, which is not conserved in eIF4GI. The figure was created using ESPrpt.⁵⁰

Superposition of the AA boxes of the four proteins revealed that residue E862 (within the AA1 box; blue arrow in Fig. 2) is conserved in all three proteins that bind eIF2 β and is replaced by K1557 in eIF4GI. These residues are exposed from the loop between α 6 and α 7. We suggest that this residue contributes to the selectivity for binding to eIF2 β .

The caspase cleavage site of DAP5/p97 is located in an unstructured loop

Activation of caspases during the process of apoptosis leads to the cleavage of DAP5/p97 at

DETD⁷⁹² positioned at its C-terminus (Fig. 2). This cleavage was shown by biochemical studies to activate some properties of DAP5/p97 in cells. A corresponding cleavage site was not observed for eIF4GI, eIF2B ϵ , and eIF5. Indeed, based on sequence and structure alignment, DAP5-CTD exhibits extra residues in this region (Fig. 2). Interestingly, our structure of DAP5-CTD has missing electron density between residues 789 and 795, which contains the cleavage site. This is an inherent property of DAP5-CTD, as electron density in this region is not observed in both independent crystallographic monomers (see Supplementary Fig. 1). Protease

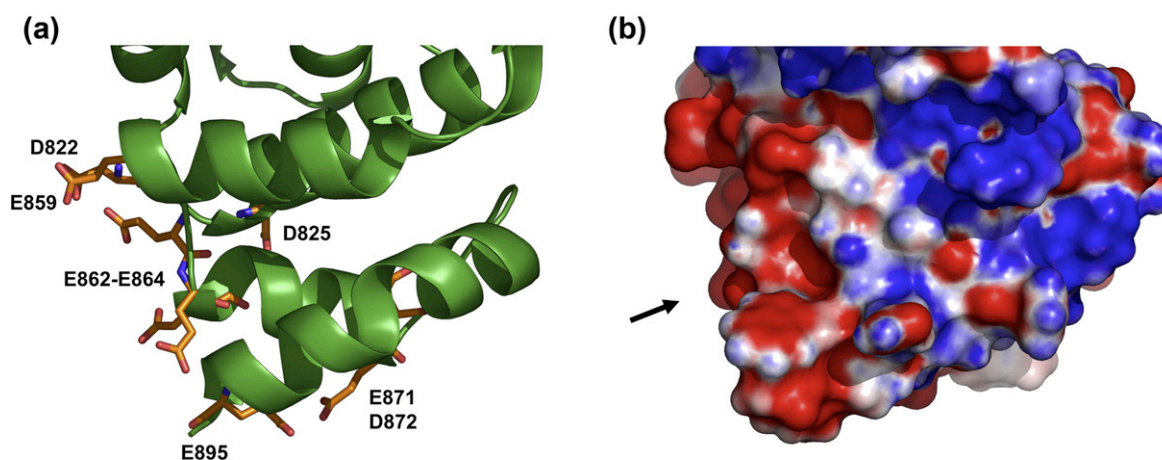


Fig. 3. Acidic residues form an electron-negative patch on DAP5-CTD. (a) The acidic residues in the two AA boxes (E859, E862, E863, E864, E871, D872, and E895) together with exposed residues from a loop connecting α 4 and α 5 (D822 and E825), drawn as sticks in orange. (b) Electrostatic surface representation [same view as in (a)] showing the electronegative patch (red) formed by these residues, indicated by an arrow.

cleavage sites, in general, and caspase cleavage sites, in particular, are often located in flexible, unstructured regions of proteins, in agreement with our missing density.⁴⁰ Indeed, several structures have been solved for caspase substrates, revealing that the site of cleavage is within a disordered mobile loop whose structure is not resolved.⁴⁰ In eIF4GI, eIF2B ϵ , and eIF5, which lack the caspase cleavage site, this region is structured and characterized by a short loop connecting helices $\alpha 3$ and $\alpha 4$ (illustrated by comparing this region in eIF4GI in Fig. 4a). Notably, the structure also shows that DHVD⁸²⁵, the other putative cleavage site, is completely structured (Fig. 2). Moreover, this segment is part of helix $\alpha 5$ that is unlikely to undergo cleavage; thus, the structure is in line with a previous mutation analysis¹⁸ showing that this site is not cleaved.

Upon cleavage of DAP5/p97, the C-terminal fragment is removed, yielding an active DAP5/p86 isoform.¹⁸ Indeed, the structure shows that helices $\alpha 4$ – $\alpha 8$ form very few interactions with the remaining protein, thus allowing for its release upon caspase cleavage. To illustrate this, we have defined two segments of DAP5-CTD in the vicinity of the cleavage site: segment A between residues 730 and 788 ($\alpha 1$ – $\alpha 3$), and segment B between residues 796 and 897 ($\alpha 4$ – $\alpha 8$). Interestingly, in DAP5-CTD, there are only 15 atom–atom contacts up to 3.5 Å between the two segments, whereas in the CTDs of eIF4GI, eIF2B ϵ , and eIF5, there are 42, 53, and 49 atom–atom contacts, respectively. The small number of interactions between the two segments of DAP5-CTD is in agreement with the fact that DAP5-CTD loses segment B upon caspase cleavage. Table 2 summarizes the residues involved in the atom–atom interactions between the two segments for DAP5-CTD and eIF4GI (with the latter representing the trend observed for eIF2B ϵ and eIF5). In both proteins, all the interactions between the two

Table 2. Interactions (up to 3.5 Å) between side chains in segments A and B in the C-terminal domains of DAP5-CTD and eIF4GI (italicized residues designate interactions in the loop between $\alpha 3$ and $\alpha 4$)

Interacting helices	DAP5 ^a		eIF4GI ^b	
	A (730–788)	B (796–897)	A (1441–1495)	B (1496–1566)
$\alpha 1$ – $\alpha 4$			S1456	R1508
$\alpha 2$ – $\alpha 4$	P747	S811	N1458	A1507 R1508
$\alpha 2$ – $\alpha 4$	Y751	K818		
$\eta 1$ – $\alpha 5$			V1475	K1521
$\alpha 3$ – $\alpha 5$	K766	D825 S829		
$\alpha 3$ – $\alpha 4$			L1479	Y1515
$\alpha 3$ – $\alpha 5$			V1480	K1521
$\alpha 3$ – $\alpha 5$			M1484	A1525
$\alpha 3$ – $\alpha 6$			C1488	F1546
$\alpha 3$ – $\alpha 4$			A1491	D1501
$\alpha 3$ – $\alpha 5$	S781	H837		
$\alpha 3$ – $\alpha 4$			I1493	R1499 L1498
$\alpha 3$ – $\alpha 4$	E783	Q804	F1494	L1498
$\alpha 3$ – $\alpha 4$	V784	Q801	<i>E1495</i>	T1496 <i>P1497</i> <i>L1498</i> <i>R1499</i>
$\alpha 3\alpha 4$	N785	Q801		

^a According to DAP5-CTD structure PDB entry 3D3M based on Fig. 2.

^b Numbering according to eIF4G structure PDB entry 1UG3.

segments involve residues either from $\alpha 3$ or from $\alpha 4$ (except for $\eta 1$ – $\alpha 5$ in the case of eIF4GI). Notably, in DAP5-CTD, there are only three pairs of interacting residues between $\alpha 3$ and $\alpha 4$, weakly holding the two helices (Fig. 4b). On the other hand, in eIF4GI, there are many interactions primarily located at the loop, while one is at the bottom edge of the two helices stabilizing the interaction between $\alpha 3$ and $\alpha 4$ (Fig. 4c and Table 2). Thus, the lack of density in the loop region of DAP5-CTD and the few interactions

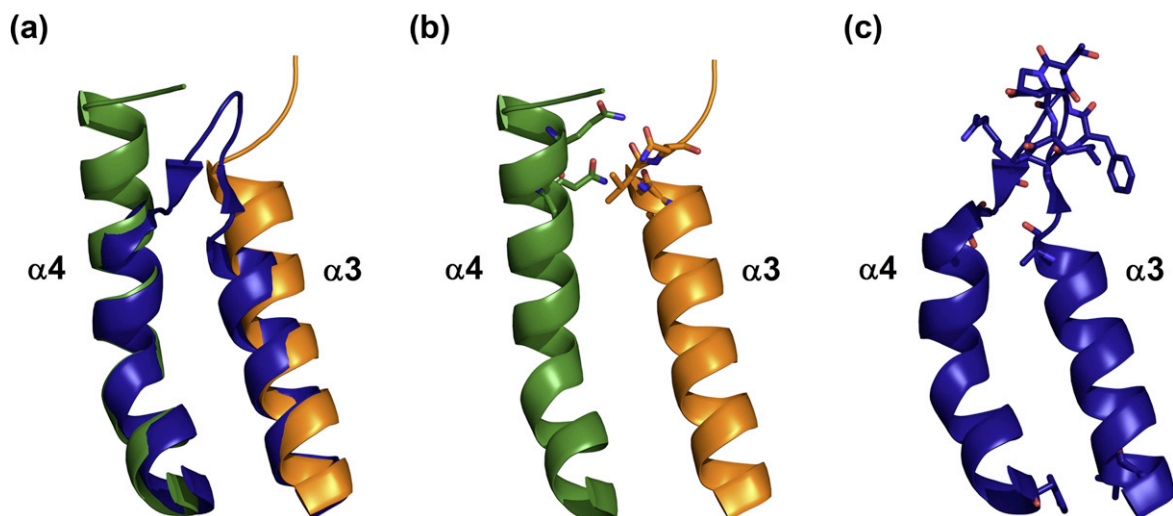


Fig. 4. $\alpha 3$ and $\alpha 4$ flanking the loop containing the caspase cleavage site of DAP5-CTD in comparison to the corresponding region in eIF4GI. (a) Superposition of $\alpha 3$ (orange) and $\alpha 4$ (green) of DAP5-CTD to those of eIF4GI (blue). (b) Interacting residues between $\alpha 3$ and $\alpha 4$ of DAP5-CTD (up to 3.5 Å) and (c) between $\alpha 3$ and $\alpha 4$ of eIF4GI (up to 3.5 Å).

between its flanking helices support biochemical studies showing that this loop contains its unique protease cleavage site.

It appears that DAP5-CTD is composed of two subdomains (segments A and B) that are loosely held together. Removal of segment B from DAP5-CTD exposes a hydrophobic surface, which harbors

an elongated groove where helix $\alpha 4$ (residues 812–819) is situated (Fig. 5a and b). This putative hydrophobic surface is a “sticky” region that may be adequate for forming protein–protein interactions, assuming that the conformation is retained. It is noteworthy that helix $\alpha 4$ has a proline in position 814 and is therefore kinked, leaving its imprint on

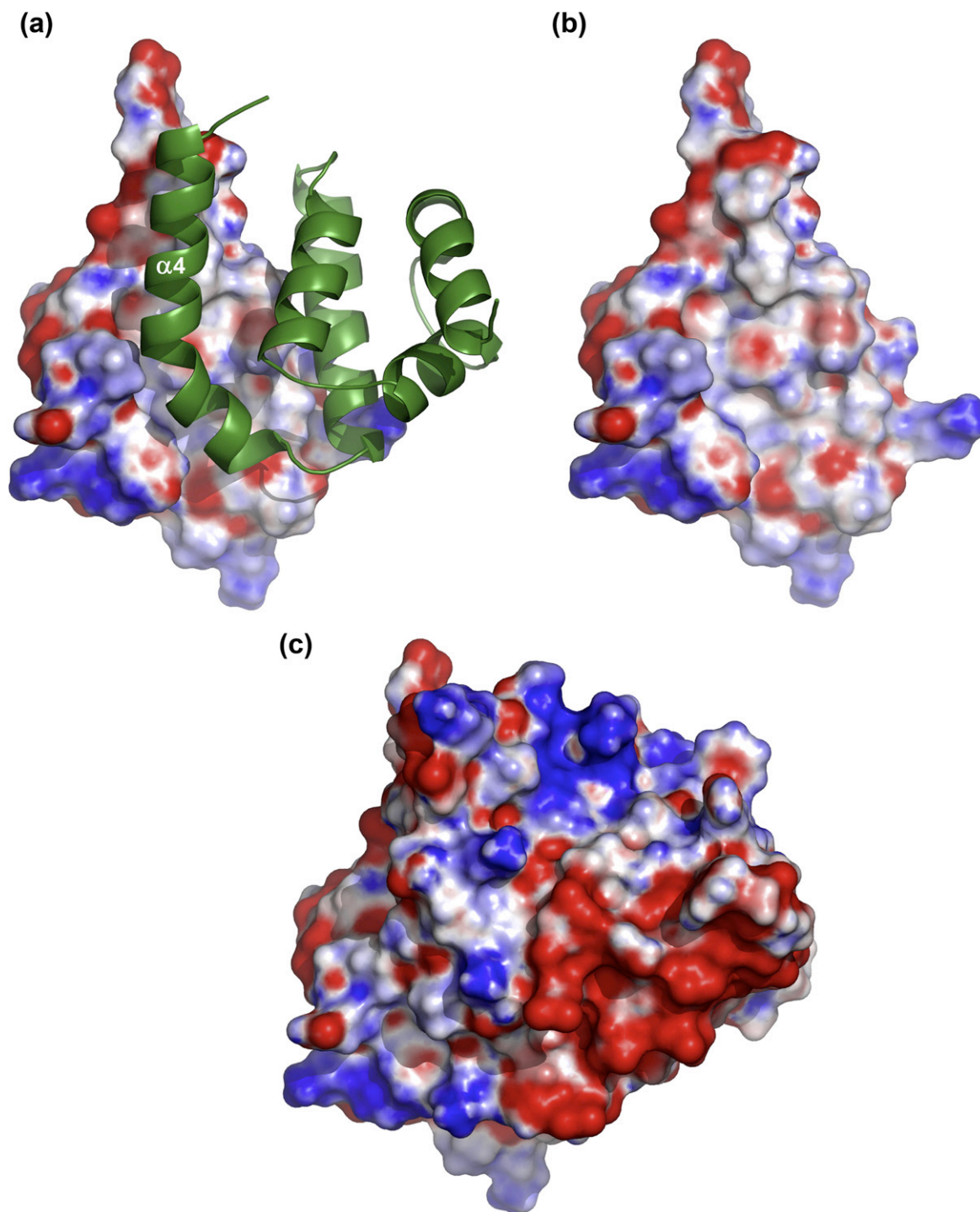


Fig. 5. Electrostatic surface representation of DAP5-CTD. (a) Electrostatic surface representation of segment A (residues 730–788) with segment B (residues 796–897) shown in green ribbon; $\alpha 4$ is indicated. (b) The exposed hydrophobic surface of segment A revealed upon removal of segment B. (c) Electrostatic surface representation of DAP5-CTD showing the negative patch located in segment B [same view as in (a) and (b)].

the hydrophobic groove. Taken together, two major structural changes occur upon the removal of segment B by the caspase cleavage. The protein loses its negatively charged C-terminus (Fig. 5c) and, as a result, may lose its ability to bind to Mnk1 and eIF2 β . At the same time, a new hydrophobic surface is exposed in the truncated p86 isoform, suggesting the acquisition of an alternative repertoire of interaction partners. Notably, in the full-length protein, α 4 interferes with possible access to this hydrophobic groove. This suggests that segment B may have an autoinhibitory effect on such possible interactions in the context of the full-length protein.

Materials and Methods

Expression and purification of selenomethionine recombinant DAP5-CTD

DAP5-CTD (730–898) was cloned into pET28-TEVH⁴¹ and expressed as an N-terminal 6 \times His fusion. BL21(DE3) bacteria expressing pET28-His-TEV-DAP5-CTD were grown at 37 °C in M9 minimal medium containing glucose (0.4% wt/vol) and kanamycin (30 μ g/ml). At A_{600} =0.6, selenomethionine (50 mg/L), along with lysine hydrochloride (100 mg/L), threonine (100 mg/L), phenylalanine (100 mg/L), leucine (50 mg/L), isoleucine (50 mg/L), and valine (50 mg/L), were added as solid. Protein expression was induced by the addition of 100 μ M isopropyl-1-thio- β -D-galactopyranoside for 24 h at 15 °C. Bacteria were lysed by sonication in 50 mM Tris-HCl (pH 8), 500 mM NaCl, and 1 mM PMSF and protease inhibitor cocktail (Calbiochem) in the presence of DNase (1 μ g/ml) and lysosyme (40 U/ml). Soluble protein was purified using a Ni-NTA column (HiTrap chelating HP; GE Healthcare), followed by gel-filtration chromatography (HiLoad 16/60 Superdex 75; GE Healthcare) in 50 mM Tris (pH 7.0), 150 mM NaCl, and 1 mM DTT. Pooled fractions containing purified DAP5-CTD were then concentrated to 40 mg/ml for crystallization experiments.

Crystallization, data collection, and refinement

Crystals of DAP5-CTD were obtained by the microbatch method, under oil, using the Oryx6 robot (Douglas Instruments Ltd., East Garston, Hungerford, Berkshire, UK). Selenomethionine DAP5-CTD crystals were grown from a precipitating solution of 100 mM MMT (D,L-maleic acid, 4-morpholineethanesulfonic acid, and Tris; pH 6) and 20% polyethylene glycol 1500. Crystals formed in space group $P2_1$ with cell constants a =61.06 Å, b =45.73 Å, c =63.36 Å, and β =103.8°, and contained two monomers in the asymmetric unit cell with a V_m of 2.17 Å³/Da. The multiple-wavelength anomalous diffraction data from a single crystal were collected at European Synchrotron Radiation Facility beamline BM14. Data up to 1.9 Å resolution were collected at peak and remote wavelengths. The diffraction images were indexed and integrated using the program HKL2000.⁴² Integrated reflections were scaled using the program SCALEPACK.⁴² Structure factor amplitudes were calculated using TRUNCATE from the CCP4 program suite.⁴³ Details of the data collection are described in Table 1. Selenium sites were identified with the programs SHELX⁴⁴ and HKL2MAP.⁴⁵

All steps of atomic refinement were carried out with the program CCP4/Refmac5.⁴⁶ Calculations of overall anisotropic temperature factors and noncrystallographic symmetry restraints were used throughout all steps of refinement. The model was built to $2F_{\text{obs}} - F_{\text{calc}}$ and $F_{\text{obs}} - F_{\text{calc}}$ maps using the program Coot.⁴⁷ In later rounds of refinement, water molecules were built into peaks greater than 3σ in $F_{\text{obs}} - F_{\text{calc}}$ map. The current model contains residues 730–788, residues 796–897, and 75 water molecules. The R_{free} value is 27.3% (for 5% of the reflections not used in the refinement), and the R_{work} value is 22.9% for all data up to 1.9 Å. The DAP5-CTD model was evaluated with the program PROCHECK.⁴⁸ Details of the refinement statistics of the DAP5-CTD structure are described in Table 1. All figures depicting structures were prepared using PyMOL.⁴⁹ Manual structure alignment was performed using the Homology module of InsightII (Accelrys, Inc., San Diego, CA). The figure illustrating the sequence alignment was prepared using ESPript.⁵⁰

Accession code

The coordinates and structure factors for DAP5-CTD have been deposited in RCSB PDB under accession no. 3D3M.

Acknowledgements

We are grateful to Prof. Joel L. Sussman for his helpful discussions. We thank Dr. Heinz Gut at European Synchrotron Radiation Facility beamline BM14. Part of this work was supported by the Israel Science Foundation (A.K.). The structure was determined at the Israel Structural Proteomics Center, supported by The Israel Ministry of Science, Culture, and Sport; the Divadol Foundation; the Neuman Foundation; the Pearl Foundation; and the European Commission Sixth Framework Research and Technological Development Program 'SPINE2-COMPLEXES' Project (under contract no. 031220) and 'Teach-SG' Project (under contract no. ISSG-CT-2007-037198). A.K. is the incumbent Helena Rubinstein Chair of Cancer Research.

Supplementary Data

Supplementary data associated with this article can be found, in the online version, at doi:10.1016/j.jmb.2008.08.013

References

1. Mader, S., Lee, H., Pause, A. & Sonenberg, N. (1995). The translation initiation factor eIF-4E binds to a common motif shared by the translation factor eIF-4 gamma and the translational repressors 4E-binding proteins. *Mol. Cell. Biol.* **15**, 4990–4997.
2. Sonenberg, N. & Dever, T. E. (2003). Eukaryotic translation initiation factors and regulators. *Curr. Opin. Struct. Biol.* **13**, 56–63.

3. Rogers, G. W., Jr, Komar, A. A. & Merrick, W. C. (2002). eIF4A: the godfather of the DEAD box helicases. *Prog. Nucleic Acid Res. Mol. Biol.* **72**, 307–331.
4. Pyronnet, S., Imataka, H., Gingras, A. C., Fukunaga, R., Hunter, T. & Sonenberg, N. (1999). Human eukaryotic translation initiation factor 4G (eIF4G) recruits mnk1 to phosphorylate eIF4E. *EMBO J.* **18**, 270–279.
5. Waskiewicz, A. J., Johnson, J. C., Penn, B., Mahalingam, M., Kimball, S. R. & Cooper, J. A. (1999). Phosphorylation of the cap-binding protein eukaryotic translation initiation factor 4E by protein kinase Mnk1 *in vivo*. *Mol. Cell. Biol.* **19**, 1871–1880.
6. Hellen, C. U. & Sarnow, P. (2001). Internal ribosome entry sites in eukaryotic mRNA molecules. *Genes Dev.* **15**, 1593–1612.
7. Jackson, R. J. (2005). Alternative mechanisms of initiating translation of mammalian mRNAs. *Biochem. Soc. Trans.* **33**, 1231–1241.
8. Pestova, T. V., Kolupaeva, V. G., Lomakin, I. B., Pilipenko, E. V., Shatsky, I. N., Agol, V. I. & Hellen, C. U. (2001). Molecular mechanisms of translation initiation in eukaryotes. *Proc. Natl Acad. Sci. USA*, **98**, 7029–7036.
9. Marash, L. & Kimchi, A. (2005). DAP5 and IRES-mediated translation during programmed cell death. *Cell Death Differ.* **12**, 554–562.
10. Prevot, D., Darlix, J. L. & Ohlmann, T. (2003). Conducting the initiation of protein synthesis: the role of eIF4G. *Biol. Cell*, **95**, 141–156.
11. Imataka, H., Olsen, H. S. & Sonenberg, N. (1997). A new translational regulator with homology to eukaryotic translation initiation factor 4G. *EMBO J.* **16**, 817–825.
12. Marcotrigiano, J., Lomakin, I. B., Sonenberg, N., Pestova, T. V., Hellen, C. U. & Burley, S. K. (2001). A conserved HEAT domain within eIF4G directs assembly of the translation initiation machinery. *Mol. Cell*, **7**, 193–203.
13. Morino, S., Imataka, H., Svitkin, Y. V., Pestova, T. V. & Sonenberg, N. (2000). Eukaryotic translation initiation factor 4E (eIF4E) binding site and the middle one-third of eIF4GI constitute the core domain for cap-dependent translation, and the C-terminal one-third functions as a modulatory region. *Mol. Cell. Biol.* **20**, 468–477.
14. Imataka, H., Gradi, A. & Sonenberg, N. (1998). A newly identified N-terminal amino acid sequence of human eIF4G binds poly(A)-binding protein and functions in poly(A)-dependent translation. *EMBO J.* **17**, 7480–7489.
15. Lamphear, B. J., Kirchweger, R., Skern, T. & Rhoads, R. E. (1995). Mapping of functional domains in eukaryotic protein synthesis initiation factor 4G (eIF4G) with picornaviral proteases. Implications for cap-dependent and cap-independent translational initiation. *J. Biol. Chem.* **270**, 21975–21983.
16. Levy-Strumpf, N., Deiss, L. P., Berissi, H. & Kimchi, A. (1997). DAP-5, a novel homolog of eukaryotic translation initiation factor 4G isolated as a putative modulator of gamma interferon-induced programmed cell death. *Mol. Cell. Biol.* **17**, 1615–1625.
17. Gradi, A., Imataka, H., Svitkin, Y. V., Rom, E., Raught, B., Morino, S. & Sonenberg, N. (1998). A novel functional human eukaryotic translation initiation factor 4G. *Mol. Cell. Biol.* **18**, 334–342.
18. Henis-Korenblit, S., Strumpf, N. L., Goldstaub, D. & Kimchi, A. (2000). A novel form of DAP5 protein accumulates in apoptotic cells as a result of caspase cleavage and internal ribosome entry site-mediated translation. *Mol. Cell. Biol.* **20**, 496–506.
19. Imataka, H. & Sonenberg, N. (1997). Human eukaryotic translation initiation factor 4G (eIF4G) possesses two separate and independent binding sites for eIF4A. *Mol. Cell. Biol.* **17**, 6940–6947.
20. Asano, K., Krishnamoorthy, T., Phan, L., Pavitt, G. D. & Hinnebusch, A. G. (1999). Conserved bipartite motifs in yeast eIF5 and eIF2Bepsilon, GTPase-activating and GDP-GTP exchange factors in translation initiation, mediate binding to their common substrate eIF2. *EMBO J.* **18**, 1673–1688.
21. Asano, K., Shalev, A., Phan, L., Nielsen, K., Clayton, J., Valasek, L. *et al.* (2001). Multiple roles for the C-terminal domain of eIF5 in translation initiation complex assembly and GTPase activation. *EMBO J.* **20**, 2326–2337.
22. Bellsolle, L., Cho-Park, P. F., Poulin, F., Sonenberg, N. & Burley, S. K. (2006). Two structurally atypical HEAT domains in the C-terminal portion of human eIF4G support binding to eIF4A and Mnk1. *Structure*, **14**, 913–923.
23. Boesen, T., Mohammad, S. S., Pavitt, G. D. & Andersen, G. R. (2004). Structure of the catalytic fragment of translation initiation factor 2B and identification of a critically important catalytic residue. *J. Biol. Chem.* **279**, 10584–10592.
24. Lee, S. H. & McCormick, F. (2006). p97/DAP5 is a ribosome-associated factor that facilitates protein synthesis and cell proliferation by modulating the synthesis of cell cycle proteins. *EMBO J.* **25**, 4008–4019.
25. Shaughnessy, J. D., Jr, Jenkins, N. A. & Copeland, N. G. (1997). cDNA cloning, expression analysis, and chromosomal localization of a gene with high homology to wheat eIF-(iso)4F and mammalian eIF-4G. *Genomics*, **39**, 192–197.
26. Yamanaka, S., Poksay, K. S., Arnold, K. S. & Innerarity, T. L. (1997). A novel translational repressor mRNA is edited extensively in livers containing tumors caused by the transgene expression of the apoB mRNA-editing enzyme. *Genes Dev.* **11**, 321–333.
27. Henis-Korenblit, S., Shani, G., Sines, T., Marash, L., Shohat, G. & Kimchi, A. (2002). The caspase-cleaved DAP5 protein supports internal ribosome entry site-mediated translation of death proteins. *Proc. Natl Acad. Sci. USA*, **99**, 5400–5405.
28. Nevins, T. A., Harder, Z. M., Korneluk, R. G. & Holcik, M. (2003). Distinct regulation of internal ribosome entry site-mediated translation following cellular stress is mediated by apoptotic fragments of eIF4G translation initiation factor family members eIF4GI and p97/DAP5/NAT. *J. Biol. Chem.* **278**, 3572–3579.
29. Warnakulasuriyachchi, D., Cerquozzi, S., Cheung, H. H. & Holcik, M. (2004). Translational induction of the inhibitor of apoptosis protein HIAP2 during endoplasmic reticulum stress attenuates cell death and is mediated via an inducible internal ribosome entry site element. *J. Biol. Chem.* **279**, 17148–17157.
30. Hundsdoerfer, P., Thoma, C. & Hentze, M. W. (2005). Eukaryotic translation initiation factor 4GI and p97 promote cellular internal ribosome entry sequence-driven translation. *Proc. Natl Acad. Sci. USA*, **102**, 13421–13426.
31. Lewis, S. M., Cerquozzi, S., Graber, T. E., Ungureanu, N. H., Andrews, M. & Holcik, M. (2007). The eIF4G homolog DAP5/p97 supports the translation of select mRNAs during endoplasmic reticulum stress. *Nucleic Acids Res.* **36**, 168–178.

32. Mikami, S., Masutani, M., Sonenberg, N., Yokoyama, S. & Imataka, H. (2006). An efficient mammalian cell-free translation system supplemented with translation factors. *Protein Expression Purif.* **46**, 348–357.
33. Nousch, M., Reed, V., Bryson-Richardson, R. J., Currie, P. D. & Preiss, T. (2007). The eIF4G-homolog p97 can activate translation independent of caspase cleavage. *RNA*, **13**, 374–384.
34. Marash, L., Liberman, N., Henis-Korenblit, S., Sivan, G., Reem, E., Elroy-Stein, O. & Kimchi, A. (2008). DAP5 promotes cap-independent translation of Bcl-2 and CDK1 to facilitate cell survival during mitosis. *Mol. Cell*, **30**, 447–459.
35. Bieniossek, C., Schutz, P., Bumann, M., Limacher, A., Uson, I. & Baumann, U. (2006). The crystal structure of the carboxy-terminal domain of human translation initiation factor eIF5. *J. Mol. Biol.* **360**, 457–465.
36. Prilusky, J., Felder, C. E., Zeev-Ben-Mordehai, T., Rydberg, E. H., Man, O., Beckmann, J. S. *et al.* (2005). FoldIndex: a simple tool to predict whether a given protein sequence is intrinsically unfolded. *Bioinformatics*, **21**, 3435–3438.
37. Perry, J. & Kleckner, N. (2003). The ATRs, ATMs, and TORs are giant HEAT repeat proteins. *Cell*, **112**, 151–155.
38. Preiss, T. & Hentze, W. M. (2003). Starting the protein synthesis machine: eukaryotic translation initiation. *BioEssays*, **25**, 1201–1211.
39. Das, S. & Maitra, U. (2000). Mutational analysis of mammalian translation initiation factor 5 (eIF5): role of interaction between the beta subunit of eIF2 and eIF5 in eIF5 function *in vitro* and *in vivo*. *Mol. Cell. Biol.* **20**, 3942–3950.
40. Timmer, J. C. & Salvesen, G. S. (2007). Caspase substrates. *Cell Death Differ.* **14**, 66–72.
41. Peleg, Y. & Unger, T. (2008). Application of high-throughput methodologies to the expression of recombinant proteins in *E. coli*. In *Methods in Molecular Biology. Structural Proteomics: High-Throughput Methods* (Kobe, B., Guss, M. & Huber, T., eds), vol. 426, pp. 197–208, Humana Press, Totowa, NJ.
42. Otwinowski, Z. & Minor, W. (1997). Processing of X-ray diffraction data collected in oscillation mode. *Methods Enzymol.* **276**, 307–326.
43. French, G. S. & Wilson, K. S. (1978). On the treatment of negative intensity observations. *Acta Crystallogr. Sect. A*, **34**, 517–525.
44. Sheldrick, G. (1998). SHELX: applications to macromolecules. In *Direct Methods for Solving Macromolecular Structures* (Fortier, S., ed), pp. 401–411, Kluwer Academic Publishers, Dordrecht.
45. Pape, T. & Schneider, T. R. (2004). HKL2MAP: a graphical user interface for phasing with SHELX program. *J. Appl. Crystallogr.* **37**, 843–844.
46. Murshudov, G. N., Vagin, A. A. & Dodson, E. J. (1997). Refinement of macromolecular structures by the maximum-likelihood method. *Acta Crystallogr. Sect. D*, **53**, 240–255.
47. Emsley, P. & Cowtan, K. (2004). Coot: model-building tools for molecular graphics. *Acta Crystallogr. Sect. D*, **60**, 2126–2132.
48. Laskowski, R. A., MacArthur, M. W. & Moss, D. S. (1993). PROCHECK: a program to check the stereochemical quality of protein structures. *J. Appl. Crystallogr.* **26**, 283–291.
49. DeLano, W. L. (2002). *The PyMOL Molecular Graphics System*. DeLano Scientific, San Carlos, CA, USA; <http://www.pymol.org>
50. Gouet, P., Courcelle, E., Stuart, D. I. & Metz, F. (1999). ESPript: analysis of multiple sequence alignments in PostScript. *Bioinformatics*, **15**, 305–308.